# Global phase diagram of three-dimensional extended Boson Hubbard model: A continuous-time quantum Monte Carlo study

Bin Xi,[1] Fei Ye,[2] Weiqiang Chen,[3] Fuchun Zhang,[3] and Gang Su[1,*]

[1]*College of Physical Sciences, Graduate University of Chinese Academy of Sciences, Beijing 100049, China*

[2]*College of Material Sciences and Optoelectric Technology, Graduate University of Chinese Academy of Sciences, Beijing 100049, China*

[3]*Centre of Theoretical and Computational Physics and Department of Physics, the University of Hong Kong, Hong Kong, China*

(Received 27 March 2011; revised manuscript received 23 June 2011; published 8 August 2011)

We present the global phase diagram of the extended boson Hubbard model on a simple cubic lattice by quantum Monte Carlo simulation with the worm update algorithm. Four kinds of phases are supported by this model, including superfluid, supersolid, Mott, and charge density wave (CDW) states, which are identified in the phase diagram of chemical potential $\mu$ versus nearest-neighbor interaction $V$. By changing the chemical potential, a continuous transition is found from the Mott phase to a superfluid phase without breaking the translational symmetry. For an insulating CDW state, adding particles to it gives rise to a continuous transition to a supersolid phase, while removing particles usually leads to a first-order transition to either a supersolid or superfluid phase. By tuning the nearest-neighbor interaction, one can realize the transition between two insulating phases, Mott and CDW, with the same particle density, which turns out to be first order. We also confirm the result in Phys. Rev. B 79, 094503 (2009) that a supersolid phase with average particle density less than $1/2$ can exist in a small region of the $\mu$-$V$ phase diagram.

DOI: 10.1103/PhysRevB.84.054512 PACS number(s): 67.80.kb, 75.40.Mg, 02.60.−x, 64.60.−i

## I. INTRODUCTION

Lattice models of interacting bosons and fermions such as the Hubbard model and its various generalizations are usually strongly correlated systems exhibiting various phases with competing orders, which are of fundamental interest in fields of both condensed matter and cold atomic physics. Interests in both types of Hubbard models have been renewed recently since they can be realized in cold atomic gases loaded in optical lattices (for a review see Refs. [1] and [2] and references therein). Unlike fermions, there is a natural superfluid order for free bosons at zero temperature driven by the kinetic energy. When the interaction is switched on, the bosons are likely to be localized in various crystalline patterns, which may coexist with superfluid order[3–6] to give a realization of an intriguing "supersolid" state that has been pursued since the 1950s.[7–10] Recently, people have observed the nonclassical rotational inertia in solidified $^4$He,[11,12] implying a possible supersolid state, which, in spite of the controversy over this topic, has also triggered extensive studies on various boson Hubbard models.

Experimentally, the boson Hubbard model can be used to mimic granular superconductors, where the Cooper pairs are described as bosons and which has been studied by Fisher *et al.*[13] two decades ago. With only an onsite repulsive interaction, they showed that bosons can form either a Mott insulating state with integer filling or a superfluid state. Such a Mott-superfluid transition has been studied extensively with various numerical methods.[14–19] Recent experimental progress in a cold atomic system provides another realization of the boson Hubbard model by loading atoms into an optical lattice with possible long-range interactions through the dipole interaction[20–22] or mediated by other intermediate states or fermions.[23–25] In addition, the boson models also share similarities with quantum magnets; for example, the uniaxial magnetization corresponds to insulating states of the boson Hubbard model (see, e.g., Ref. [26]), while the easy-plane magnetization corresponds to the superfluid state. Hence, the studies on the boson Hubbard model may shed light on some common issues of strongly correlated lattice models.

Generally speaking, boson models with interactions at zero temperature have two principal phases: (i) the superfluid and (ii) the incompressible insulating state, which are favored respectively by kinetic and interaction energies and can coexist. Depending on the features of the interaction terms, there are several types of insulating phases, such as Mott, valence bond crystal, and charge density wave (CDW). Note that, in this article, we define the incompressible states with oscillating density profile as CDW, although the bosons may not carry charges.

The extended boson Hubbard (EBH) model with onsite $U$ and nearest-neighbor $V$ interactions is a minimal model in favor of CDW and supersolid phases, which has the form

$$\hat{H} = -t\sum_{\langle i,j\rangle}(\hat{b}_i^\dagger \hat{b}_j + \hat{b}_j^\dagger \hat{b}_i) + \frac{U}{2}\sum_i \hat{n}_i(\hat{n}_i - 1) + V\sum_{\langle i,j\rangle}\hat{n}_i\hat{n}_j - \mu\sum_i \hat{n}_i, \quad (1)$$

where $\hat{b}_i^\dagger$ ($\hat{b}_i$) is the creation (annihilation) bosonic operator at site $i$, $t$ is the hopping amplitude, $\hat{n}_i = \hat{b}_i^\dagger\hat{b}_i$ is the particle number, $\mu$ is the chemical potential, and $\langle i,j\rangle$ runs over all nearest neighbors. Recently, Hamiltonian Eq. (1) and its hard-core version (equivalent to the quantum spin-$1/2$ $XXZ$ model) with different underlying lattices have been extensively studied in different parameter regimes.[5,6,27–34] However, a global phase diagram of the three-dimensional (3D) EBH model [Eq. (1)] is still lacking. Because there is no sign problem for the EBH model, the quantum Monte Carlo (QMC) simulation is the most convenient tool for this purpose. The

 

worm algorithm[35–37] will be invoked to study Hamiltonian (1) on a simple cubic lattice, together with other perturbation and mean-field approaches.

The system described by the EBH model can give rise to a charge-ordered crystal at commensurate fillings. The first one is for half filling $\rho = 0.5$, and the corresponding solid state is labeled CDW I. Doping particles into this state can lead to a supersolid state.[5,6] However, as shown in Ref. [5], doping holes into it makes it act quite differently, which may not result in a supersolid state with $\rho < 0.5$, but in a phase separation between superfluid and CDW I states, which signals a first-order phase transition. Their argument is based on the two following observations: (i) Taking one particle out of a perfect CDW crystal with half filling costs almost no potential energy but only chemical potential. At the same time, the hopping hole also gains a kinetic energy which is quadratic in $t$ ($\sim t^2$). For a perfect CDW crystal, these three processes are balanced, so one cannot take one particle out. (ii) The CDW phase breaks the translational symmetry, leading to a twofold degenerate ground state. If holes are doped into the domain wall between these two degenerate phases, the kinetic energy gained is proportional to $t$. Hence, the CDW phase is unstable toward domain wall formation if the hole density exceeds $L^{-1}$ for an $L^d$ lattice, although it is still stable against losing one particle. This argument perfectly explains the first-order phase transition from the CDW I to the superfluid state with $\rho \leqslant 0.5$, but it fails in two circumstances. The first is that, in one dimension, the kinetic energy is always linear in $t$, and the corresponding transition is of the Kosterlitz-Thouless type.[6] The other is that, if $V$ is comparable to $t$, the kinetic energy of holes is also linear in $t$, which may result in the supersolid phase with the particle density less than half filling (see Sec. II B). This can be verified by mean-field calculations.[32,38]

At unitary filling, the ground state can be either a uniform Mott insulator with one particle per site or a charge-ordered crystal with two particles on one sublattice and empty on the other one which is labeled CDW II. There is a critical region around $U \sim zV$, where the two states with different translation symmetries become degenerate; however, they are separated thermodynamically (i.e., any local perturbation cannot take one to the other). Correspondingly, the transition between them is a first-order transition. Note that the aforementioned transition from the superfluid to CDW I state by tuning the chemical potential is weak first order.[27] Far less attention has been paid to the region with $zV \sim U$ by now, of which the details are given as part of the phase diagram in this article. To plot the ground-state phase diagram, we focus on the case with small hopping and average particle density near to or smaller than 1. For larger $t$ or $\rho$, we expect essentially no new physics.

This article is organized as follows. In Sec. II, we shall present the global phase diagram. The details of the order parameters will be discussed in Sec. III. The conclusion will be given in the last section.

## II. GLOBAL PHASE DIAGRAM

### A. Classical case with $t = 0$

We start from the classical case without hopping. The energy per site of the ground state is a function of the particle numbers on the two sublattices $n_A$ and $n_B$:

$$\epsilon^{(0)}(n_A,n_B) = -\frac{\mu}{2}(n_A + n_B) + \frac{zV}{2}n_A n_B + \frac{U}{4}[n_A(n_A - 1) + n_B(n_B - 1)], \quad (2)$$

where the coordination number $z = 6$ for the simple cubic lattice. The states can be labeled by $(n_A,n_B)$. The Mott states correspond to $n_A = n_B$, and the CDW states with $n_A \neq n_B$ break the translational symmetry, which is twofold degenerate. In this article, we define the state (1,0) as the CDW I state and (2,0) as the CDW II state and, for convenience, we only consider $n_A > n_B$ for the CDW states.

For $\mu < 0$ the ground state is a vacuum without any particles. As the chemical potential is increased ($\mu > 0$), the particles are loaded into one sublattice to form a charge-ordered pattern with $n_A = 1$ and $n_B = 0$ (i.e., the CDW I state). If we further increase the chemical potential, more particles are loaded into the cubic lattice, which fill either the empty sites if $zV/U < 1$ to form a uniform Mott state or the occupied sites if $zV/U > 1$, leading to a CDW II state. In the Mott state, each particle interacts with its nearest neighbors, which effectively lowers the chemical potential to $\mu - zV$, and then the critical line between the CDW I and Mott states is simply $\mu = zV$. The critical line between the CDW I and II states is a horizontal line $\mu = U$ because the chemical potential only needs to compensate the onsite interaction $U$ for adding new particles.

Similarly, by studying the instability of adding particle to a state $(n_A,n_B)$, one can determine all the phase boundaries between different classical insulating states, as shown in Fig. 1. There is a special vertical line $zV/U = 1$, on which many states can coexist with the same free energy. For example, on the boundary between the Mott and CDW II states, there are actually three macroscopic states, which are (1,1), (2,0), and (0,2). In fact, some of them only exist on this line in the absence of hopping terms; for example, states (3,1) and (1,3) on the boundary between the Mott (2,2) and CDW (4,0) states. These degenerate states are macroscopic and cannot be smoothly

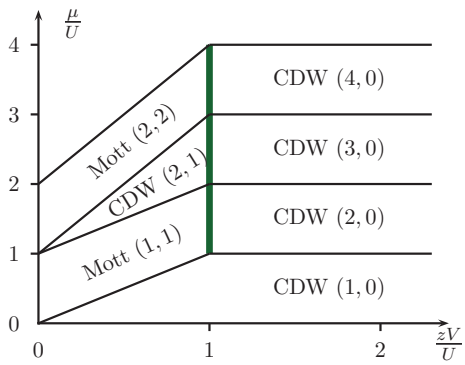


FIG. 1. (Color online) Phase diagram with zero hopping $t = 0$, where the states are labeled by the particle numbers on two sublattices $(n_A,n_B)$ with the assumption $n_A \geqslant n_B$. The states with $n_A < n_B$ can be obtained by inversion. The CDW states with one sublattice empty on the right side. Some states can only exist on the thick solid green line; for example, states (3,1) and (1,3).

transformed into each other by local perturbations (i.e., there are infinitely high barriers between these macroscopic states).

### B. Case for finite $t$

For the case with finite hopping $t$, the particles (holes) adding to an insulating state can gain kinetic energy, which results in the shrinking of insulating areas in the phase diagram (Fig. 2) compared with the classical case (Fig. 1). In three dimensions, these mobile bosons condense at low temperature, leading to superfluidity, which enriches the phase diagram. There are four phases for the EBH model characterized by the following three quantities: the particle density $\rho$, the superfluid density $\rho_s$,[39] and the solid structure factor $S_{\vec{\pi}}$ at momentum $\vec{\pi} = (\pi,\pi,\pi)$ with

$$\rho_s = m\langle W_x^2 + W_y^2 + W_z^2\rangle/(3\beta L),$$
$$S_{\vec{\pi}} = \frac{1}{N^2}\sum_{\vec{r},\vec{r}'} e^{-i\vec{\pi}\cdot(\vec{r}-\vec{r}')}\langle n_{\vec{r}} n_{\vec{r}'}\rangle, \tag{3}$$

where $W_x$, $W_y$, and $W_z$ are the winding numbers along the $x$, $y$, and $z$ directions, respectively, $\beta$ is the inverse temperature, and $m = 1/(2t)$ is the effective mass of the bosons. In the insulating Mott and CDW states, particles are localized by the interaction and the local particle number is quantized as in the classical case. The pure superfluid state has nonzero

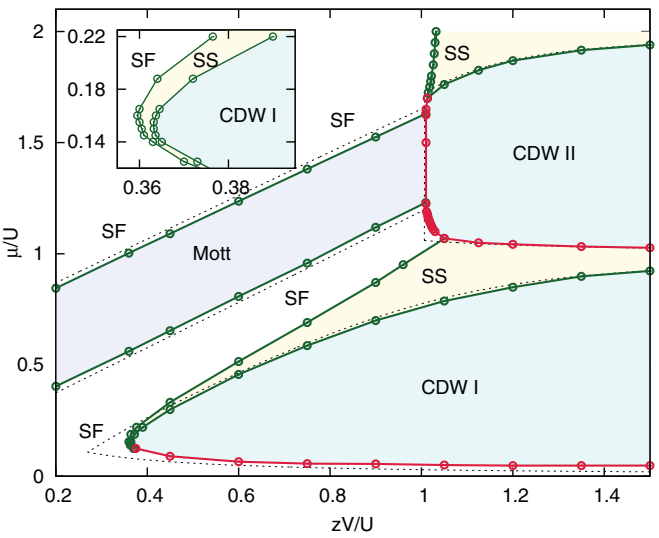


FIG. 2. (Color online) The phase diagram in the $\mu/U$ vs $zV/U$ plane for the extended Bose Hubbard model on a simple cubic lattice, where $U = 40t$ and the lattice size is $12 \times 12 \times 12$. Four kinds of phases including the superfluid (SF), supersolid (SS), Mott, and CDW states are identified. The CDW states are further classified as I and II by the filling numbers. The solid lines with circles are the phase boundaries calculated by QMC simulations, and the dotted lines are from the perturbation calculations. The green lines are second-order phase boundaries, and the red lines are first order. The inset is a zoom near the tip of the CDW I lobe, where one can find a narrow region below the lobe corresponding to a supersolid phase with the filling less than one half. For details of order parameters one may refer to Figs. 5 and 6.

superfluid density $\rho_s$ and a vanishing solid structure factor $S_{\vec{\pi}}$, while both are finite in the supersolid phase.

Figure 2 is the phase diagram determined by the QMC simulation with the worm update algorithm, where the solid lines with circles are the QMC results and the dotted lines are from the perturbation expansion in the strong-coupling limit[31] where the insulating states become unstable against adding or removing particles. It is seen that the perturbation results agree quite well with those of the QMC simulation in part of the phase diagram, but it is still not applicable in some regions since it cannot deal with the superfluid order.

Compared with the classical case in Fig. 1, the CDW I state is detached from its insulating neighbors (i.e., the Mott, CDW II, and vacuum states). The upper boundary of the vacuum state is actually lowered below $\mu = 0$ due to the hopping of bosons, which is not shown in Fig. 1. The gaps between the different insulating states are filled with the superfluid and supersolid phases. The lower boundary of the CDW I state is a critical line on which there occurs a phase separation between the superfluid and CDW I phases, which breaks the U(1) gauge symmetry and the translational symmetry, respectively. The transition between them is weak first order, across which the particle density and superfluid density exhibit a jump. Considering the correspondence between the EBH model and spin models, this transition is similar to the spin-flopping process in the two- or three-dimensional anisotropic $XXZ$ model in the presence of a magnetic field pointing along the $z$ axis, which is equivalent to the EBH model in the hard-core limit.[40–42] As explained in Ref. [5], this first-order phase transition with a particle-number jump is due to the fact that the CDW I phase is unstable toward the domain wall formation if the filling number exceeds $L^{-1}$, although it is still stable against doping one hole.

Doping particles upon the CDW I phase by increasing the chemical potential does not lead to a first-order transition as in the hard-core EBH model (or equivalently the $XXZ$ model), where the particle-hole symmetry makes the upper and lower boundaries of the CDW I phase identical. In the case of soft-core bosons, these additional particles can move upon the alternating charge-ordered background with the effective hopping amplitude $t^2$, which can Bose condense at zero temperature without destroying the staggered-density order, and thus leads to a supersolid state with $\rho > 0.5$. This transition is second order, as shown by the solid green line in Fig. 2 where all the second-order phase boundaries are green to distinguish them from the first-order phase boundaries, which are red.

Continuously increasing the chemical potential upon the supersolid phase, two different situations occur: (1) For $zV < U$, the particles like to occupy the empty sites, which weakens the CDW order and is accompanied by the occurrence of superfluid order. Until some critical filling $\rho < 1$, the CDW order is completely destroyed and a pure superfluid state appears with the translational symmetry restored. The transition is second order. (2) For $zV > U$, the additional particles are added to the occupied sites so that the CDW order is actually enhanced until finally entering into another insulating state (i.e., CDW II) through a first-order phase transition, for which the reason is the same as that from the superfluid with $\rho < 0.5$ to CDW I. In this sense, the

staggered-density order in supersolid phase is inherited from the CDW I state and is not related to the CDW II state, since doping holes into the CDW II state cannot smoothly result in the supersolid state.

As shown in a previous study,[5] doping holes into the CDW I state may not lead to the supersolid state with $\rho < 0.5$ on a two-dimensional square lattice, contrary to the case of doping particles. The reason is that the CDW I state has twofold degeneracy. As long as enough particles are removed, the insulating state becomes unstable toward the formation of domain walls between the two degenerate states, but can still be stable against losing one particle. This explains the particle-density jump across the first-order phase boundary between the superfluid and CDW I phases and that between the supersolid and CDW II phases. However, this argument is invalid for $V$ close to $t$ that is around the tip of the CDW I lobe, where we show below that the kinetic energy gain by doping one hole into the CDW I state is also linear in $t$, which can cause instability of the CDW I state toward a supersolid state without the formation of domain walls. Suppose that one particle is taken from a CDW I state; the hole left behind moves in an effective staggered potential, which is, roughly speaking, 0 in one sublattice and $(z-2)V$ in the other. Solving this single-particle problem, one estimates that the kinetic energy gain $\Delta K$ is

$$\Delta K = -tz\left[\frac{V}{2t}\left(1-\frac{2}{z}\right)+\sqrt{1+\left(\frac{V}{2t}\right)^2\left(1-\frac{2}{z}\right)^2}\right]^{-1}, \tag{4}$$

which is about $-2.88t$ in the cubic lattice near the tip of the CDW I lobe where $V \sim 2.4t$ (see Fig. 2). As a consequence, a supersolid phase with $\rho < 0.5$ occurs, whose boundary is plotted in the inset of Fig. 2. This result has already been obtained in Ref. [32] by extrapolating the QMC (stochastic series expansion method) results to the thermodynamic limit and by a mean-field calculation.

In the presence of a kinetic term, the vertical boundary at $zV \sim U$ between Mott and CDW II states does not yet split but moves slightly to the CDW side. On this boundary, the free energies of both states are equal. However, they have different symmetries and are separated from each other thermodynamically. The transition between these two insulating states is first-order, which is similar to the conventional liquid-solid phase transition. Further doping particles into the Mott and CDW II states leads to the reentrance of superfluid and supersolid states, respectively, with density $\rho > 1$.

The particles or holes can hop between nearest neighbors on a Mott background, which leads to a kinetic energy gain linear in $t$. However, they can only hop among next-nearest neighbors in a staggered-CDW background, which gives rise to a hopping energy proportional to $t^2/V$. Then, as $t$ increases, the Mott region shrinks much faster than the CDW II region, which results in the mismatch of the phase boundary between them as $zV \sim U$ (see Fig. 2). Since doping the Mott state with holes leads to a superfluid state, one expects a boundary between the superfluid state and the CDW II state in the critical region at the lower end of the vertical boundary. This phase boundary is again first order. At the upper end, the extension of the vertical boundary separates the superfluid and supersolid phases in a second-order phase transition.

## III. ORDER PARAMETERS

In this section we give the details of the parameters $\rho$, $\rho_s$, and $S_{\vec{\pi}}$ for different $\mu$ and $V$. Figure 3 is the density profile as we vary the chemical potential for several fixed values of $V$, where the plateaus correspond to the incompressible states (i.e., the Mott and CDW I and II states), with vanishing isothermal compressibility $\kappa_T \equiv \rho^{-2}\partial\rho/\partial\mu$. Note that these insulating states correspond to two single points $\rho = 0.5$ and $\rho = 1$ in Fig. 4, which is the plot of superfluid density $\rho_s$ and $S_{\vec{\pi}}$ as functions of particle density $\rho$.

For $\rho < 0.5$, the particles Bose condense to form a pure superfluid state with a nonzero $\rho_s$ but vanishing $S_{\vec{\pi}}$, as shown in Fig. 4. When the particle density reaches a commensurate value $\rho = 0.5$, a plateau appears, implying $\kappa_T = 0$, which corresponds to the incompressible CDW I state with translational invariance broken. This transition is first order since the particle density, as a first-order derivative of free energy with respect to the chemical potential, is discontinuous. This is also reflected in Fig. 4 by the fact that a segment of particle density below the half filling is inaccessible and, at $\rho = 0.5$, $S_{\vec{\pi}}$ jumps from zero to a finite value. As the particle density exceeds 0.5, $\kappa_T$ becomes a finite-positive value again. At the same time the superfluidity appears continuously on the CDW I state to form a supersolid. The corresponding transition is second order, since the particle density $\rho$ is continuous but $\kappa_T$ jumps from zero to a finite value.

Between the two plateaus at $\rho = 0.5$ and $\rho = 1$, the slope of the $\rho(\mu)$ curve for $V/t = 3$, 4, and 5 (i.e., $zV < U$), shows another jump, implying that $\kappa_T$ is discontinuous and is a second-order phase transition from the supersolid to superfluid phase. This transition is manifested in Fig. 4, where $\rho_s$ remains finite in the whole region $0.5 < \rho < 1.0$, but $S_{\vec{\pi}}$ vanishes at some critical values in between. Further increasing

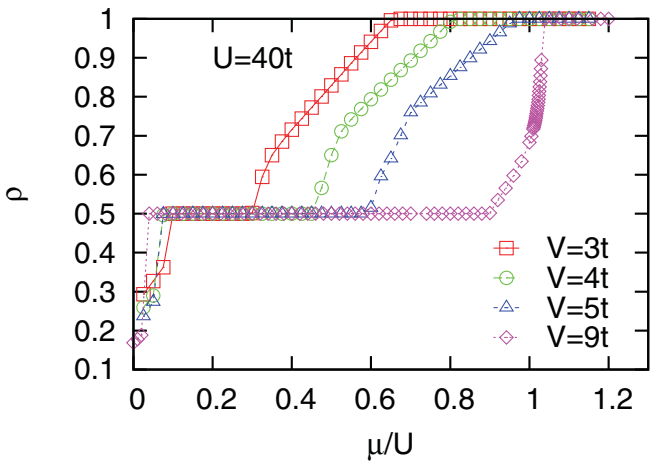


FIG. 3. (Color online) Average particle density $\rho$ as a function of chemical potential $\mu$ for different $V$ and for $U = 40t$. The first plateau at $\rho = 0.5$ corresponds to the CDW I phase, and the second one corresponds to the Mott phase for $V/t = 3,4,5$ and the CDW II phase for $V/t = 9$. The system size is $12 \times 12 \times 12$.

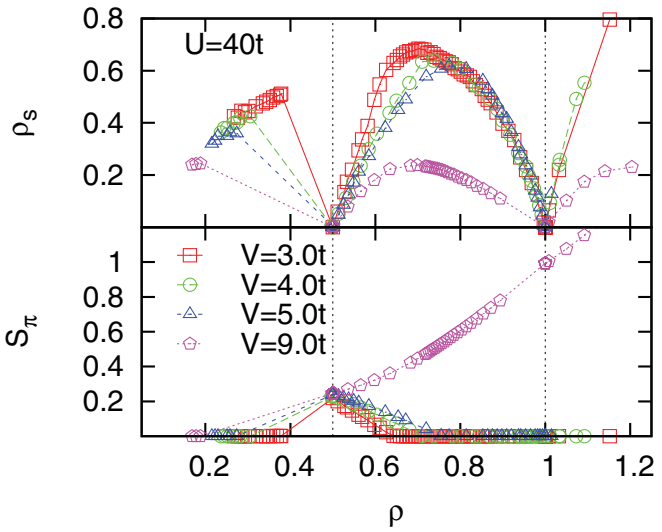


FIG. 4. (Color online) Superfluid density $\rho_s$ and solid structure factor $S_{\vec{\pi}}$ as functions of the particle density $\rho$ at $U/t = 40$. Note that the plateaus of constant $\rho$ in Fig. 3 are only single points here.

the chemical potential, the system enters the Mott phase, which corresponds to the plateau with $\rho = 1$ in Fig. 3 through a second-order phase transition. At the transition point, $\rho_s$ vanishes, as shown in Fig. 4.

For $V = 9t$ (i.e., $zV/U > 1$), the second plateaus in Fig. 3 corresponds to the CDW II state, into which the system enters directly from the supersolid phase as $\mu$ is increased. The transition is first-order, as shown in Fig. 3 by the jump in particle density. It is also reflected in Fig. 4 where a segment of particle density $\rho$ is not accessible before $\rho$ reaches 1.

In Fig. 5, we plot the rescaled order parameters $\tilde{\rho}_s \equiv \rho_s/\rho_{s,\max}$ and $\tilde{S}_{\vec{\pi}} \equiv S_{\vec{\pi}}/S_{\vec{\pi},\max}$ as functions of $zV/U$ around

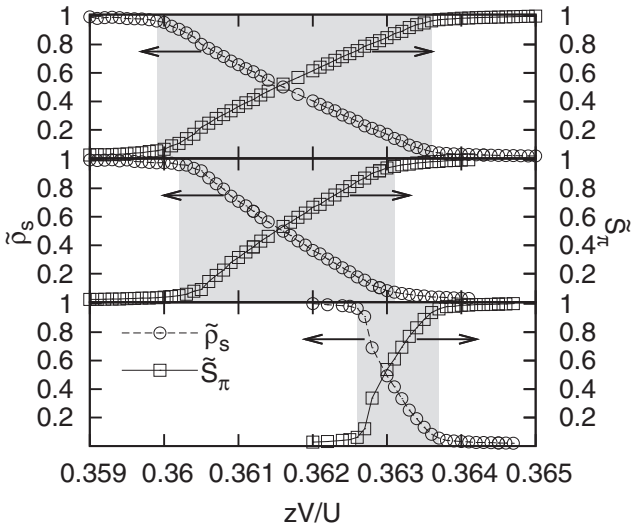


FIG. 5. Rescaled order parameters $\tilde{\rho}_s$ and $\tilde{S}_{\vec{\pi}}$ as functions of $zV/U$, which are normalized by their maxima. The upper, middle, and bottom panels correspond to $\mu/U = 0.160$, 0.155, and 0.145, respectively. The supersolid phases occur in the shaded areas. The lattice size is $12 \times 12 \times 12$.

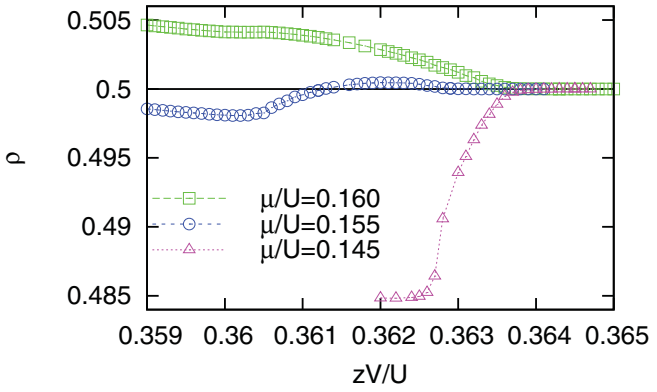


FIG. 6. (Color online) Particle density vs $zV/U$ for $\mu/U = 0.160$, 0.155, and 0.145.

the CDW I lobe, where $\rho_{s,\max} \approx 0.6$ and $S_{\vec{\pi},\max} \approx 0.2$. In the plot, we take three characteristic values of the chemical potential $\mu/U = 0.160$, 0.155, and 0.145 from the top to the bottom panel. In the shaded areas, when $V$ increases, the superfluid density $\rho_s$ decreases while the solid structure factor $S_{\vec{\pi}}$ increases, and both $\rho_s$ and $S_{\vec{\pi}}$ are nonzero in this region, indicating a supersolid state. The supersolid area becomes more and more narrow as $\mu$ decreases, until it finally shrinks to a point on the $zV/U$ axis when $\mu/U \sim 0.140$, which implies that two second-order phase boundaries merge into one first-order phase boundary across which the order parameters $\rho_s$ and $S_{\vec{\pi}}$ are both discontinuous. The corresponding density profiles are plotted in Fig. 6, where we observe that the particle density is always smaller than 0.5 for $\mu/U = 0.145$, corresponding to the bottom panel in Fig. 5, until it enters the CDW I phase, which implies that the supersolid state can exist below half filling. For $\mu/U = 0.160$, the situation is different where $\rho$ decreases as $V$ increases, which can be intuitively attributed to the loss of effective chemical potential due to the nearest-neighbor interaction $V$ in the mean-field level. The case of $\mu/U = 0.155$ shows an intermediate behavior, for which the particle number first decreases then increases slightly above 0.5 and finally reaches the CDW I state.

## IV. CONCLUSION

In this article, we present the global phase diagram (Fig. 2) of the 3D extended Bose Hubbard model. The EBH model exhibits four kinds of ground states, including (1) the Mott state without breaking any symmetry, (2) the CDW I and II states with translational symmetry broken, (3) the superfluid state with U(1) gauge symmetry broken, and (4) the supersolid state with both symmetries broken. By using a QMC simulation as well as other analytical tools, we identify the transition type between these phases. Among them, the first-order phase boundary includes the boundaries between the superfluid and CDW (I and II) states and between the Mott and CDW II states. The other boundaries are all continuous. The critical regions for $zV/U \sim 1$ and the tip of the CDW I lobe are examined in detail. We demonstrate that, in the present 3D EBH model, the supersolid phase with $\rho < 0.5$ can appear in

a small region near the CDW I lobe where the hopping amplitude $t$ is comparable to the nearest-neighbor interaction $V$. In this region, the general "domain wall" argument for the nonexistence of the supersolid state with $\rho < 0.5$ is no longer applicable, since it is based on the assumption that $t \ll V$.


## ACKNOWLEDGMENTS

We acknowledge the helpful discussions with M. Ma. This work is supported by NSFC Grants No. 10904081, No. 10934008, and No. 90922033, HKSAR RGC Grant No. HKU 701009, and the Chinese Academy of Sciences.


*gsu@gucas.ac.cn


[1] I. Bloch, J. Dalibard, and W. Zwerger, Rev. Mod. Phys. **80**, 885 (2008).
[2] H. Zhai, Frontiers of Physics in China **4**, 1 (2009).
[3] G. G. Batrouni, R. T. Scalettar, G. T. Zimanyi, and A. P. Kampf, Phys. Rev. Lett. **74**, 2527 (1995).
[4] A. van Otterlo, K.-H. Wagenblast, R. Baltin, C. Bruder, R. Fazio, and G. Schön, Phys. Rev. B **52**, 16176 (1995).
[5] P. Sengupta, L. P. Pryadko, F. Alet, M. Troyer, and G. Schmid, Phys. Rev. Lett. **94**, 207202 (2005).
[6] G. G. Batrouni, F. Hébert, and R. T. Scalettar, Phys. Rev. Lett. **97**, 087209 (2006).
[7] O. Penrose and L. Onsager, Phys. Rev. **104**, 576 (1956).
[8] A. F. Andreev and I. M. Lifshitz, Sov. Phys. JETP **29**, 1107 (1969).
[9] G. V. Chester, Phys. Rev. A **2**, 256 (1970).
[10] A. J. Leggett, Phys. Rev. Lett. **25**, 1543 (1970).
[11] E. Kim and M. H. W. Chan, Nature (London) **427**, 225 (2004).
[12] E. Kim and M. H. W. Chan, Science **305**, 1941 (2004).
[13] M. P. A. Fisher, P. B. Weichman, G. Grinstein, and D. S. Fisher, Phys. Rev. B **40**, 546 (1989).
[14] B. Capogrosso-Sansone, N. V. Prokof'ev, and B. V. Svistunov, Phys. Rev. B **75**, 134302 (2007).
[15] Y. Kato, Q. Zhou, N. Kawashima, and N. Trivedi, Nat. Phys. **4**, 617 (2008).
[16] J. K. Freericks, H. R. Krishnamurthy, Y. Kato, N. Kawashima, and N. Trivedi, Phys. Rev. A **79**, 053631 (2009).
[17] Y. Kato and N. Kawashima, Phys. Rev. E **79**, 021104 (2009).
[18] Y. Kato and N. Kawashima, Phys. Rev. E **81**, 011123 (2010).
[19] T. Sato, T. Suzuki, and N. Kawashima, Phys. Rev. A **81**, 025601 (2010).
[20] A. Griesmaier, J. Werner, S. Hensler, J. Stuhler, and T. Pfau, Phys. Rev. Lett. **94**, 160401 (2005).
[21] T. Rieger, T. Junglen, S. A. Rangwala, P. W. H. Pinkse, and G. Rempe, Phys. Rev. Lett. **95**, 173002 (2005).
[22] K.-K. Ni, S. Ospelkaus, M. H. G. de Miranda, A. Pe'er, B. Neyenhuis, J. J. Zirbel, S. Kotochigova, P. S. Julienne, D. S. Jin, and J. Ye, Science **322**, 231 (2008).
[23] H. P. Büchler and G. Blatter, Phys. Rev. Lett. **91**, 130404 (2003).
[24] V. W. Scarola and S. Das Sarma, Phys. Rev. Lett. **95**, 033003 (2005).
[25] N. Henkel, R. Nath, and T. Pohl, Phys. Rev. Lett. **104**, 195302 (2010).
[26] W. Li, S.-S. Gong, Y. Zhao, and G. Su, Phys. Rev. B **81**, 184427 (2010).
[27] A. Kuklov, N. Prokof'ev, and B. Svistunov, Phys. Rev. Lett. **93**, 230402 (2004).
[28] R. G. Melko, A. Paramekanti, A. A. Burkov, A. Vishwanath, D. N. Sheng, and L. Balents, Phys. Rev. Lett. **95**, 127207 (2005).
[29] X. Lu and Y. Yu, Phys. Rev. A **74**, 063615 (2006).
[30] S. Yi, T. Li, and C. P. Sun, Phys. Rev. Lett. **98**, 260405 (2007).
[31] M. Iskin and J. K. Freericks, Phys. Rev. A **79**, 053634 (2009).
[32] K. Yamamoto, S. Todo, and S. Miyashita, Phys. Rev. B **79**, 094503 (2009).
[33] L. Pollet, J. D. Picon, H. P. Büchler, and M. Troyer, Phys. Rev. Lett. **104**, 125302 (2010).
[34] H. T. Ueda and K. Totsuka, Phys. Rev. B **81**, 054442 (2010).
[35] N. V. Prokof'ev, B. V. Svistunov, and I. S. Tupitsyn, JETP Lett. **64**, 911 (1996).
[36] N. V. Prokof'ev, B. V. Svistunov, and I. S. Tupitsyn, Phys. Lett. A **238**, 253 (1998).
[37] V. A. Kashurnikov, N. V. Prokof'ev, B. V. Svistunov, and M. Troyer, Phys. Rev. B **59**, 1162 (1999).
[38] F. Ye *et al.* (unpublished).
[39] E. L. Pollock and D. M. Ceperley, Phys. Rev. B **36**, 8343 (1987).
[40] M. Kohno and M. Takahashi, Phys. Rev. B **56**, 3212 (1997).
[41] G. G. Batrouni and R. T. Scalettar, Phys. Rev. Lett. **84**, 1599 (2000).
[42] G. Schmid, S. Todo, M. Troyer, and A. Dorneich, Phys. Rev. Lett. **88**, 167208 (2002).